JACS
JOURNAL OF THE AMERICAN CHEMICAL SOCIETY

Article

Endohedral Hydrogen Exchange Reactions in C_{60} (*n*H@C, *n* = 1#5): Comparison of Recent Methods in a High-Pressure Cooker

Tae Bum Lee, and Michael L. McKee

J. Am. Chem. Soc., **2008**, 130 (51), 17610-17619 • DOI: 10.1021/ja8071868 • Publication Date (Web): 24 November 2008

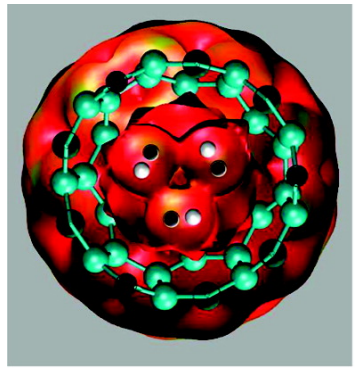

$3H_2@C_{60}$

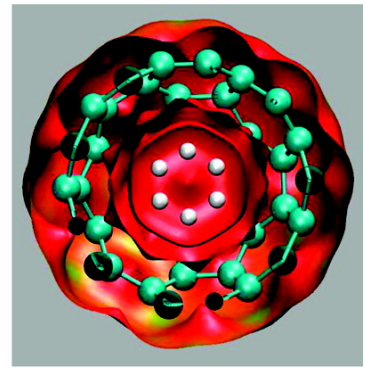

$3H_2@C_{60}TS$

More About This Article

Additional resources and features associated with this article are available within the HTML version:

- Supporting Information
- Access to high resolution figures
- Links to articles and content related to this article
- Copyright permission to reproduce figures and/or text from this article

View the Full Text HTML

J|A|C|S
ARTICLES

Published on Web 11/24/2008

Endohedral Hydrogen Exchange Reactions in C_{60} ($nH_2@C_{60}$, $n = 1-5$): Comparison of Recent Methods in a High-Pressure Cooker

Tae Bum Lee and Michael L. McKee*

Department of Chemistry and Biochemistry, Auburn University, Auburn, Alabama 36849

Received September 10, 2008; E-mail: mckee@chem.auburn.edu

Abstract: The interactions of several H_2 molecules [$(H_2)_n$, $n = 1-5$] within C_{60}, C_{70}, and C_{82} have been studied with several DFT methods as well as with MP2 and SCS-MP2. As expected, B3LYP significantly underestimates dispersion interactions, while the M05-2X and M06-2X methods are in much better agreement with MP2 and SCS-MP2 results. Degenerate hydrogen exchange reactions were calculated for $3H_2 \rightarrow 3H_2$ inside C_{60}, C_{70}, and C_{82}. The free-energy barrier at 298 K for the hydrogen exchange reaction $3H_2 \rightarrow 3H_2$ is reduced from 88.8 kcal/mol for the free reaction to 36.2 kcal/mol for the reaction within C_{60}, corresponding to a k_{cat}/k_{uncat} ratio of 10^{36}. Steric compression, dispersion, and a favorable entropy contribute similar increments to the reduction in the free-energy barrier.

Introduction

A catalyst speeds up a reaction without being consumed. Catalysts can be synthetic or natural (enzymes) and can speed up reactions by factors of 10^{18} or more.[1] In the present work, we consider the catalytic effect of C_{60} on a reaction taking place inside the cage. Reactions inside clathrates, hemicarcerands, zeolites, and other supermolecular systems have been known for some time.[2−12] For example, Donald Cram won a Nobel Prize for his work on host−guest complexes, including novel reactions that can take place inside a molecular container, an "inner phase" that represents a unique molecular environment.[7,8] Warmuth showed that several different reactions can take place inside a hemicarcerand, including the conversion of benzocyclopropenone to benzyne,[2] the rearrangement of phenylnitrene,[3] and a Diels−Alder reaction.[4]

Encapsulated guests forming neutral endohedral fullerenes are well-known.[13−67] The known and computed endrohedral complexes in C_{60} are given in Table 1. While a number of atomic endohedral complexes of C_{60} are known, insertion of molecules into the C_{60} cage has been difficult. For example, only a trace amount of N_2 (1:2000 $N_2@C_{60}/N@C_{60}$) can be formed by heating $N@C_{60}$ to 650 °C under a N_2 pressure of 3500 atm.[23] However, a significant advance was made by

Table 1. Observed and Computed (ab Initio or DFT) Endohedral C_{60} Complexes (excluding Lanthanides)

$X@C_{60}$ observed	ref	$X@C_{60}$ computed	ref
H_2	15, 16	H_2	34−37
D_2	17	$(H_2)_n$ (general)	38−44
H_2O	18	$(H_2)_n$ ($n = 1-24$)	45
Li	19	$(H_2)_n$ ($n = 1-26$)	46
N	20−22	$(H_2)_n$ ($n = 1-29$)	47, 48
N_2	23	H_2O	37
P	22, 24	$(H_2O)_n$ ($n = 1-4$)	49
He, Ar, Kr, Xe	25−31	NH_3	37
Cu	21	N, P, As	50−52
T[a]	32	N_2	35, 36, 53
NH_3	33	N_4	54
		CH_4	37, 55
		C_2H_2, C_2H_4, C_2H_6	56
		CO, HF, LiH, LiF	35
		LiF, LiCl, NaF	57
		M (M = H, Li, Na, K)	58
		M, M_2 (M = Li, Be, Mg, Ca, Al, Sc)	59
		Li_3	60
		Rg (Rg = He, Ne, Ar, Kr, Xe)	55, 61−64
		Rg_2 (Rg = He, Ne, Ar, Kr, Xe)	65
		M (M = Zn, Cd, Hg)	55
		Fe_3	66
		M_2 (M = Cr, Mo, W)	67

[a] Tritium.

(1) (a) Quinn, D. M.; Sikorski, R. S. In *Handbook of Protein Structure, Function and Methods*; John Wiley: New York, 2007; pp 340−347. (b) Wolfenden, R.; Snider, M. J. *Acc. Chem. Res.* **2001**, *34*, 938–945. (c) Fersht, A. *Structure and Mechanism in Protein Science*; W. H. Freeman: New York, 1999.
(2) Warmuth, R. *Angew. Chem., Int. Ed. Engl.* **1997**, *36*, 1347–1350.
(3) Warmuth, R.; Makomiec, S. *J. Am. Chem. Soc.* **2007**, *129*, 1233–1241.
(4) Warmuth, R. *Chem. Commun.* **1998**, 59–60.
(5) Cram, D. J.; Tanner, M. E.; Thomas, R. *Angew. Chem., Int. Ed. Engl.* **1991**, *30*, 1024–1027.
(6) Cram, D. J. *Nature* **1992**, *356*, 29–36.
(7) Maverick, E.; Cram, D. J. *Compr. Supramol. Chem.* **1996**, *2*, 367–418.
(8) *Container Molecules and Their Guests*; Cram, D. J., Cram, J. M., Eds.; Royal Society of Chemistry: Cambridge, U.K., 1997.
(9) Kaczmarek, A.; Zaleśny, R.; Bartkowiak, W. *Chem. Phys. Lett.* **2007**, *449*, 314–318.
(10) Warmuth, R. *Eur. J. Org. Chem.* **2001**, 423–437.
(11) Carrera, S. S.; Kerdelhué, J.-L.; Langenwalter, K. J.; Brown, N.; Warmuth, R. *Eur. J. Org. Chem.* **2005**, 2239–2249.
(12) Warmuth, R. *J. Inclusion Phenom. Macrocyclic Chem.* **2000**, *37*, 1–38.
(13) Balch, A. L. *Encycl. Supermol. Chem.* **2004**, 579–585.
(14) Dunsch, L.; Yang, S. *Phys. Chem. Chem. Phys.* **2007**, *9*, 3067–3081.
(15) Komatsu, K.; Murata, M.; Murata, Y. *Science* **2005**, *307*, 238–240.
(16) Murata, M.; Murata, Y.; Komatsu, K. *J. Am. Chem. Soc.* **2006**, *128*, 8024–8033.

10.1021/ja8071868 CCC: $40.75

Komatsu and co-workers[15,16] with the systematic synthesis of $H_2@C_{60}$. Hydrogen was inserted into a C_{60} derivative having a 13-membered ring, which was closed to form $H_2@C_{60}$ in four additional steps in 40% yield. The Raman spectrum of the H_2 embedded within the precursor cage has been reported: a small red shift (23 cm^{-1}) of the H_2 stretch frequency was observed.[68] The infrared spectra of *p*-H_2 and *o*-H_2, recently reported by Carravetta and co-workers,[69] showed red shifts of 90 cm^{-1} (*p*-H_2, 4161 → 4071 cm^{-1}; *o*-H_2, 4155 → 4065 cm^{-1}).

Several NMR studies of the $H_2@C_{60}$ complex have also appeared.[70−74] In a study of spin−lattice relaxation rates in $H_2@C_{60}$, it was discovered that H_2 is not insulated within the C_{60} cage but rather interacts more strongly with paramagnets than expected on the basis of distance.[74] In an extension of the procedure used to produce $H_2@C_{60}$, the synthesis of $D_2@C_{60}$ was also reported.[17] Lastly, several authors have analyzed the coupled translation−rotation motion of H_2 (and other diatomics) inside C_{60}.[75−78]

The interactions between multiple H_2 molecules within C_{60} have attracted attention in the literature. Türker and Erkoç[45] packed C_{60} with up to 24 H_2 molecules, and others[46] managed 26 H_2 molecules before rupturing the cage. However, the semiempirical methods used by Türker and Erkoç[41,45] have come under attack by Dodziuk[39,42] and Dolgonos.[40] Pupysheva et al.[48] [using plane-wave density functional theory (DFT) with norm-conserving pseudopotentials] reported the repulsion when 29 H_2 molecules were packed into C_{60} (this process is endothermic by >2000 kcal/mol). Dodziuk[39] (using the MM+ force field) calculated that enclosing two H_2 molecules inside C_{70} is exothermic by 3.0 kcal/mol and enclosing three H_2 molecules inside C_{80} is exothermic by 3.8 kcal/mol. The C_{60} cage can be considered as a high-pressure reaction vessel where reactions of the endohedral substrate can take place. Perhaps the simplest chemical transformation, namely, the conversion of *ortho*-hydrogen to *para*-hydrogen (*o*-$H_2@C_{60}$ → *p*-$H_2@C_{60}$) has just been demonstrated by Turro et al.[73] Another chemical transformation was demonstrated in silico by Frenking:[65] the dimerization of two atoms inside C_{60}, where two noble gas atoms larger than Ne inside a C_{60} cage can be considered to have a bond enforced by steric constraints. In this work, we have considered the simplest reaction involving exchanges of atoms, namely, the hydrogen exchange reaction $nH_2 \rightarrow nH_2$, $n = 2-5$. The actual reaction can be monitored by using one D_2 in place of one H_2 (i.e., $nH_2 + D_2 \rightarrow (n-1)H_2 + 2HD$, $n = 1-4$). In this paper, we will explore the hydrogen exchange in isolation at high levels of theory for $2H_2$ and $3H_2$. Inside C_{60}, we compare second-order Møller−Plesset perturbation theory (MP2) and spin-component-scaled MP2 (SCS-MP2) with several DFT methods that have recently been developed to better describe dispersion effects.

Computational Methods

The Gaussian03 program system[79] was used to optimize geometries at the B3LYP/6-31G(d,p) and M05-2X/6-31G(d,p)[80−83] levels of theory. A tighter SCF criterion and the Ultrafine integration mesh were used on single-point calculations. The CCSD(T)/cc-pVTZ optimizations and frequency calculations for the free $2H_2$ and $3H_2$ transition states used internal coordinates and finite-difference derivatives. The ORCA program[84] (version 2.6.4) was used for the RI-SCS-MP2/cc-pVDZ calculations,[85,86] while the NWChem5.0 program[87] was used for the M06-2X/cc-pVDZ calculations.[88,89] Basis set superposition errors (BSSEs) were corrected by using the standard counterpoise method.[90] The pressure inside C_{60} due to the H_2 molecules was calculated using the method of Pupysheva et al.[48] In this method, the component of the force $\mathbf{F}_k$ on the *k*th carbon atom along the vector $\mathbf{R}_k$ pointing toward the center of mass (CoM) of C_{60} with the hydrogen atoms removed (F_k^{perp}) is summed over all of the carbon positions; the pressure *P* is then computed as the total summed force divided by the area *A* inside C_{60}, where $A = 4\pi R^2$ is computed as the surface area of a sphere whose radius *R* is equal to the average distance of the carbon atoms to the CoM reduced by 1.2 Å to account for the inaccessible volume inside the nanocage (eq 1):

$$F_k^{\mathrm{perp}} = \frac{\mathbf{F}_k \cdot \mathbf{R}_k}{R}$$

$$P = -\frac{\sum_{k=1}^{60} F_k^{\mathrm{perp}}}{A} = -\frac{\sum_{k=1}^{60} \mathbf{F}_k \cdot \mathbf{R}_k}{4\pi R^3}$$

$$R = \langle R_k \rangle - 1.2\ \text{Å} \qquad (1)$$

Pressures are reported in gigapascals (1 GPa ≈ 10^4 atm).

Results and Discussion

The free hydrogen exchange reactions of $2H_2$ and $3H_2$ through symmetric transition states (D_{4h} and D_{6h}) are classic examples

(17) Tanabe, F.; Murata, M.; Murata, Y.; Komatsu, K. *Nippon Kagakkai Koen Yokoshu* **2006**, *86*, 1282.
(18) For H_2O in an opened C_{60} cage, see: Iwamatsu, S.; Uozaki, T.; Kobayashi, K.; Re, S.; Nagase, S.; Murata, S. *J. Am. Chem. Soc.* **2004**, *126*, 2668–2669.
(19) Gromov, A.; Krawez, N.; Lassesson, A.; Ostrovskii, D. I.; Campbell, E. E. B. *Curr. Appl. Phys.* **2002**, *2*, 51.
(20) (a) Murphy, T. A.; Pawlik, T.; Weidinger, A.; Höhne, M.; Alcala, R.; Spaeth, J.-M. *Phys. Rev. Lett.* **1996**, *77*, 1075. (b) Knapp, C.; Dinse, K.-P.; Pietzak, B.; Waiblinger, M.; Weidinger, A. *Chem. Phys. Lett.* **1997**, *272*, 433.
(21) Knapp, C.; Weiden, N.; Dinse, K.-P. *Magn. Reson. Chem.* **2005**, *43*, S199–S204.
(22) Waiblinger, M.; Lips, K.; Harneit, W.; Weidinger, A.; Dietel, E.; Hirsch, A. *Phys. Rev. B* **2001**, *64*, 159901(E)
(23) (a) Peres, T.; Cao, B. P.; Cui, W. D.; Khong, A.; Cross, R. J.; Saunders, M.; Lifshitz, C. *Int. J. Mass Spectrom.* **2001**, *210*, 241–247. (b) Suetsuna, T.; Dragoe, N.; Harneit, W.; Weidinger, A.; Shimotani, H.; Ito, S.; Takagi, H.; Kitazawa, K. *Chem.−Eur. J.* **2002**, *8*, 5079–5083. Erratum: Suetsuna, T.; Dragoe, N.; Harneit, W.; Weidinger, A.; Shimotani, H.; Ito, S.; Takagi, H.; Kitazawa, K. *Chem.−Eur. J.* **2002**, *9*, 598.
(24) Knapp, C.; Weiden, N.; Kass, K.; Dinse, K. P.; Pietzak, B.; Waiblinger, M.; Weidinger, A. *Mol. Phys.* **1998**, *95*, 999.
(25) Guha, S.; Nakamoto, K. *Coord. Chem. Rev.* **2005**, *249*, 1111–1132.
(26) (a) Weiske, T.; Wong, T.; Kraetschmer, W.; Terlouw, J. K.; Schwarz, H. *Angew. Chem., Int. Ed. Engl.* **1992**, *31*, 183–185. (b) Giblin, D. E.; Gross, M. L.; Saunders, M.; Jimenez-Vazquez, H.; Cross, R. J. *J. Am. Chem. Soc.* **1997**, *119*, 9883–9890.
(27) (a) DiCamillo, B. A.; Hettich, R. L.; Guiochon, G.; Compton, R. N.; Saunders, M.; Jimenez-Vazquez, H. A.; Khong, A.; Cross, R. J. *J. Phys. Chem.* **1996**, *100*, 9197–9201. (b) Brink, C.; Hvelplund, P.; Shen, H.; Jimenez-Vazquez, H. A.; Cross, R. J.; Saunders, M. *Chem. Phys. Lett.* **1998**, *286*, 28–34. Errata: Brink, C.; Hvelplund, P.; Shen, H.; Jimenez-Vazquez, H. A.; Cross, R. J.; Saunders, M.; *Chem. Phys. Lett.* **1998**, *290*, 551−557.
(28) Ito, S.; Takeda, A.; Miyazaki, T.; Yokoyama, Y.; Saunders, M.; Cross, R. J.; Takagi, H.; Berthet, P.; Dragoe, N. *J. Phys. Chem. B* **2004**, *108*, 3191–3195.
(29) Cross, R. J.; Khong, A.; Saunders, M. *J. Org. Chem.* **2003**, *68*, 8281–8283.
(30) Saunders, M.; Cross, R. J.; Jimenez-Vazquez, H. A.; Shimshi, R.; Khong, A. *NATO ASI Ser., Ser. C* **1996**, *485*, 449–457.
(31) Saunders, M.; Cross, R. J. *Putting nonmetals into fullerenes, Developments in Fullerene Science*; Kluwer: Dordrecht, The Netherlands, 2002; pp 1−11.
(32) Khong, A.; Cross, R. J.; Saunders, M. *J. Phys. Chem. A* **2000**, *104*, 3940–3943.
(33) For NH_3 in an opened C_{60} cage, see: Whitener, K. E., Jr.; Frunzi, M.; Iwamatsu, S.-I.; Murata, S.; Cross, R. J.; Saunders, M. *J. Am. Chem. Soc.* **2008**, *130*, 13996–13999.
(34) Ramachandran, C. N.; Roy, D.; Sathyamurthy, N. *Chem. Phys. Lett.* **2008**, *461*, 87–92.
(35) Cioslowski, J. *J. Am. Chem. Soc.* **1991**, *113*, 4139–4141.

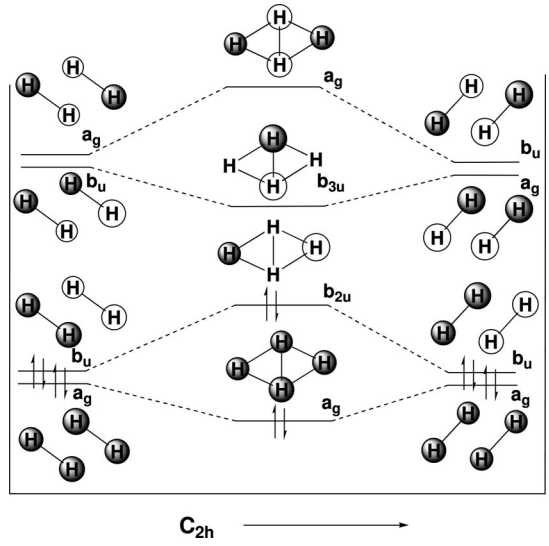

Figure 1. Correlation diagram for the hydrogen exchange reaction $2H_2 \rightarrow 2H_2$ through a C_{2h} reaction path. In contrast to a D_{2h} reaction path (not shown), the hydrogen exchange reaction along the C_{2h} path is symmetry-allowed.

of Woodward−Hoffmann-forbidden and -allowed reactions, respectively.[91] Hydrogen exchange through a bimolecular process should be strongly entropically favored over a termolecular process. While hydrogen exchange through a D_{4h} transition state is symmetry-forbidden, it is allowed through a C_{2h} reaction coordinate and a rhombic transition state (D_{2h}), as illustrated by the orbital correlation diagram in Figure 1. Gimarc[92] considered similar symmetry arguments for the bimolecular hydrogen exchange and noted the allowed transformation from the trans to the rhombic arrangements.

In 1977, Dixon, Stevens, and Herschbach[93] reported state-of-the-art calculations (DZP+CI) for both reactions through symmetric transition states. Their analysis, which included zero-point corrections (ZPC), found the barrier to be 75.8 kcal/mol, and the enthalpy of concert (i.e., the difference in enthalpy between the H−H bond enthalpy and the concerted-hydrogen-exchange activation barrier) was 25.7 kcal/mol (including ZPC). In 1989, Taylor, Kormornicki, and Dixon[94] revised the hydrogen exchange barrier. By combining the results of a full CI calculation using a DZP basis set with those of a second-order CI calculation using a large ANO basis set plus Davidson's correction, the authors estimated the energy barrier to be 66.9 kcal/mol (without ZPC) at FCI/ANO. Schleyer and co-workers[95] obtained a similar value of 68.8 kcal/mol at the QCISD(T)/6-311++G(d,2p)//MP2/6-311++G(d,2p) level of theory. They found that the enthalpy of concert for $3H_2$ was 28.3 kcal/mol (ΔH, 0 K) and concluded that the $3H_2$ transition state was significantly aromatic.

The rearrangements through the bimolecular (D_{2h}) and termolecular (D_{6h}) transition states were optimized at the B3LYP/6-31G(d,p) and CCSD(T)/cc-pVTZ levels. The first method was chosen because it was the method used for the reactions inside C_{60}, while the second method was expected to provide fairly accurate geometries and vibrational frequencies. All of the methods yielded similar results (Table 2). At the highest level of theory [CCSD(T)/cc-pVQZ//CCSD(T)/cc-pVTZ], the bimolecular and termolecular exchange reactions have barriers (ΔH, 0 K) of 106.6 and 73.1 kcal/mol, respectively. The free energies of activation at 298 K are 111.2 and 84.6 kcal/mol. The enthalpy of activation (ΔH, 0 K) for the bimolecular reaction is slightly greater than the bond enthalpy (ΔH, 0 K) of $H_2 + 2H$ (enthalpy of concert = −3.8 kcal/mol), while the enthalpy of activation (ΔH, 0 K) for the termolecular

(36) Slanina, Z.; Pulay, P.; Nagase, S. *J. Chem. Theory Comput.* **2006**, *2*, 782–785.
(37) Shameema, O.; Ramachandran, C. N.; Sathyamurthy, N. *J. Phys. Chem. A* **2006**, *110*, 2–4.
(38) Koi, N.; Oku, T. *Solid State Commun.* **2004**, *131*, 121–124.
(39) Dodziuk, H. *Chem. Phys. Lett.* **2005**, *410*, 39–41.
(40) Dolgonos, G. *THEOCHEM* **2005**, *723*, 239–241.
(41) Turker, L.; Erkoc, S. *Chem. Phys. Lett.* **2006**, *426*, 222–223.
(42) Dodziuk, H. *Chem. Phys. Lett.* **2006**, *426*, 224–225.
(43) Ren, Y. X.; Ng, T. Y.; Liew, K. M. *Carbon* **2006**, *44*, 397–406.
(44) Williams, C. I.; Whitehead, M. A.; Pang, L. *J. Phys. Chem.* **1993**, *97*, 11652–11656.
(45) Türker, L.; Erkoç, S. *THEOCHEM* **2003**, *638*, 37–40.
(46) Soullard, J.; Santamaria, R.; Jellinek, J. *J. Chem. Phys.* **2008**, *128*, 064316.
(47) Yang, C.-K. *Carbon* **2007**, *45*, 2445–2458.
(48) Pupysheva, O. V.; Farajian, A. A.; Yakobson, B. I. *Nano Lett.* **2008**, *8*, 767–774.
(49) Ramachandran, C. N.; Sathyamurthy, N. *Chem. Phys. Lett.* **2005**, *410*, 348–351.
(50) BelBruno, J. J. *Fullerenes, Nanotubes, Carbon Nanostruct.* **2002**, *10*, 23–35.
(51) Mauser, M.; Hommes, N. J. R. v. E.; Clark, T.; Hirsch, A.; Pietzak, B.; Weidinger, A.; Dunsch, L. *Angew. Chem., Int. Ed. Engl.* **1997**, *36*, 2835–2838.
(52) Kobayashi, K.; Nagase, S.; Dinse, K.-P. *Chem. Phys. Lett.* **2003**, *377*, 93–98.
(53) Slanina, Z.; Nagase, S. *Mol. Phys.* **2006**, *104*, 3167–3171.
(54) Ren, X.-Y.; Liu, Z.-Y. *Struct. Chem.* **2005**, *16*, 567–570.
(55) Pyykkö, P.; Wang, C.; Straka, M.; Vaara, J. *Phys. Chem. Chem. Phys.* **2007**, *9*, 2954–2958.
(56) Jin, L.; Zhang, M.; Su, Z.; Shi, L. *J. Theor. Comput. Chem.* **2008**, *7*, 1–11.
(57) Cioslowski, J.; Nanayakkara, A. *Phys. Rev. Lett.* **1992**, *69*, 2871–2773.
(58) Santos, J. D.; Longo, E.; Banja, M. E.; Espinoza, V. A. A.; Taft, C. A. *Int. J. Quantum Chem.* **2005**, *102*, 302–312.
(59) Zhao, Y.; Heben, M. J.; Dillon, A. C.; Simpson, L. J.; Blackburn, J. L.; Dorn, H. C.; Zhang, S. B. *J. Phys. Chem. C* **2007**, *111*, 13275–13279.
(60) Slanina, Z.; Uhlík, F.; Lee, S.-L.; Adamowicz, L.; Nagase, S. *Chem. Phys. Lett.* **2008**, *463*, 121–123.
(61) (a) Son, M.-S.; Sung, Y. K. *Chem. Phys. Lett.* **1995**, *245*, 113–118. (b) Bühl, M.; Patchkovskii, S.; Thiel, W. *Chem. Phys. Lett.* **1997**, *275*, 14–18. (c) Darzynkiewicz, R. B.; Scuseria, G. E. *J. Phys. Chem. A* **1997**, *101*, 7141–7144.
(62) Albert, V. V.; Sabin, J. R.; Harris, F. E. *Int. J. Quantum Chem.* **2007**, *107*, 3061–3066.
(63) Yan, H.; Yu, S.; Wang, X.; He, Y.; Huang, W.; Yang, M. *Chem. Phys. Lett.* **2008**, *456*, 223–226.
(64) Cioslowski, J.; Fleischmann, E. D. *J. Chem. Phys.* **1991**, *94*, 3730–3734.
(65) Krapp, A.; Frenking, G. *Chem.—Eur. J.* **2007**, *13*, 8256–8270.
(66) Gao, G.; Kang, H. S. *Chem. Phys. Lett.* **2008**, *462*, 72–74.
(67) Infante, I.; Gagliardi, L.; Scuseria, G. *J. Am. Chem. Soc.* **2008**, *130*, 7459–7465.
(68) Rafailov, P. M.; Thomsen, C.; Bassil, A.; Komatsu, K.; Bacsa, W. *Phys. Status Solidi B* **2005**, *242*, R106–R108.
(69) Mamone, S.; Ge, M.; Hüvonen, D.; Nagel, U.; Danquigny, A.; Cuda, F.; Grossel, M. C.; Murata, Y.; Komatsu, K.; Levitt, M. H.; Rõõm, T.; Carravetta, M. 2008, arXiv:0807.1589v1. arXiv.org e-Print archive. http://arxiv.org/abs/0807.1589v1 (accessed Nov 7, 2008).
(70) Sartori, E.; Ruzzi, M.; Turro, N. J.; Decatur, J. D.; Doetschman, D. C.; Lawler, R. G.; Buchachenko, A. L.; Murata, Y.; Komatsu, K. *J. Am. Chem. Soc.* **2006**, *128*, 14752–14753.
(71) Carravetta, M.; Danquigny, A.; Mamone, S.; Cuda, F.; Johannessen, O. G.; Heinmaa, I.; Panesar, K.; Stern, R.; Grossel, M. C.; Horsewill, A. J.; Samoson, A.; Murata, M.; Murata, Y.; Komatsu, K.; Levitt, M. H. *Phys. Chem. Chem. Phys.* **2007**, *9*, 4879–4894.
(72) López-Gejo, J.; Martí, A. A.; Ruzzi, M.; Jockusch, S.; Komatsu, K.; Tanabe, F.; Murata, Y.; Turro, N. J. *J. Am. Chem. Soc.* **2007**, *129*, 14554–14555.
(73) Turro, N. J.; Martí, A. A.; Chen, J. Y.-C.; Jockusch, S.; Lawler, R. G.; Ruzzi, M.; Chuang, S.-C.; Komatsu, K.; Murata, Y. *J. Am. Chem. Soc.* **2008**, *130*, 10506–10507.

Table 2. Calculated Hydrogen Exchange Barriers (kcal/mol) for $2H_2$ and $3H_2$ and Bond Dissociation Energy for H_2

	$2H_2 \rightarrow$ TS (D_{2h})[a]			$3H_2 \rightarrow$ TS (D_{6h})[b]			$H_2 \rightarrow 2H$		
	ΔE	ΔH (0 K)	ΔG (298 K)	ΔE	ΔH (0 K)	ΔG (298 K)	ΔE	ΔH (0 K)	ΔG (298 K)
B3LYP/6-31G(d,p)	103.94	105.75	110.28	61.68[c]	68.37	79.94	111.69	99.37	107.77
CCSD(T)/cc-pVTZ	105.66	106.72	111.62	67.38	73.59	85.06	108.38	102.08	110.39
CCSD(T)/cc-pVQZ[d]	105.20	106.62	111.16	66.93	73.14	84.61	109.13	102.83	111.21
DVPD+CI[e]				68.7	75.8	87.4	107.7	101.5	
SOCI+Q/ANO[f]				66.5			109.3		
QCISD(T)/6-311++G(d,2p)//MP2/6-311++G(d,2p)[g]				68.8	76.0			104.3	

[a] The imaginary frequencies at the B3LYP/6-31G(d,p) and CCSD(T)/cc-pVTZ levels are 3338i and 3188i, respectively. [b] The imaginary frequencies at the B3LYP/6-31G(d,p) and CCSD(T)/cc-pVTZ levels are 2537i and 2725i, respectively. [c] Note: ΔE(B3LYP/cc-pVDZ) is 54.99 kcal/mol. [d] Calculated for the CCSD(T)/cc-pVTZ optimized geometries and using frequencies at that level. [e] Reference 93. [f] Reference 94. [g] Reference 95.

Table 3. Sum of Second-Order NBO Interaction Energies (kcal/mol) and Number of H−H Interactions in the nH_2 Unit[a]

	sum of NBO energies (number of H−H interactions)	
n	in nH_2 cluster inside C_{60} cage	in frozen nH_2 cluster
3	11.52 (6)	12.06 (6)
4	18.62 (12)	20.68 (12)
5	20.84 (10)	22.78 (10)

[a] Donor−acceptor ($\sigma-\sigma^*$) interactions between H_2 molecules in an nH_2 cluster embedded in a C_{60} cage and as a free cluster (with frozen geometry). The number of donor−acceptor interactions is given in parentheses.

Table 4. Pressure (GPa) inside the Endohedral C_{60} Cage[a]

	B3LYP/6-31G(d,p)			M05-2X/6-31G(d,p)
n	$nH_2@C_{60}$ (TS)	$nH_2@C_{70}$ (TS)	$nH_2@C_{82}$ (TS)	$nH_2@C_{60}$ (TS)
1	0.3			−0.6
2	4.0 (3.0)			3.3 (1.9)
3	8.7 (4.8)	4.7 (1.3)	1.5 (0.4)	7.6 (2.6)
4	13.8 (9.9)			12.5 (8.0)
5	22.0 (19.2)			21.1 (18.0)

[a] Pressures for the hydrogen exchange transition states (calculated from eq 1) are given in parentheses.

reaction is 28.5 kcal/mol less than $2H_2 + 2H$ bond enthalpy (enthalpy of concert = 28.5 kcal/mol).

The donor−acceptor interactions among the H_2 molecules inside C_{60} involve the H_2 σ and σ^* orbitals. In the natural bond orbital (NBO) second-order perturbation theory analysis[96] of the Fock matrix, the summed values ($\sigma \rightarrow \sigma^*$ interactions) increase as the number of H_2 molecules increases (Table 3) and are quite large for the $5H_2$ cluster (20.8 kcal/mol). Inside C_{60}, the outward repulsive forces are balanced by the inward forces due to C_{60}. However, the donor−acceptor attractive forces remain and make the H_2 molecules act as one cluster (i.e., a single unit). The unit nH_2 ($n = 2-5$) has nearly free rotation within the cage, as revealed by one or more small (or imaginary) frequencies of the cluster within the cage. The larger frequencies (250−500 cm^{-1}) correspond to intracluster motion. Thus, one may ask whether there is H−H bonding between H_2 molecules in the cluster. This question is analogous to the question posed by Krapp and Frenking[65] of whether there is Rg−Rg bonding in $Rg_2@C_{60}$. Compression holds the H_2 molecules in positions where strong interactions are possible; whether one calls these interactions bonds or interactions may be a matter of personal choice. When an NBO analysis is carried out for $nH_2@C_{60}$ or the nH_2 cluster in a frozen geometry, the results are very similar (Table 3).

The coupling of rotations and translations of the endohedral substrate within the C_{60} cage is nontrivial.[75−78] For H_2, five additional modes exist in the endohedral complex $H_2@C_{60}$ relative to $H_2 + C_{60}$. In an oversimplification, two of these new modes are rotations while three are translations (rattling), but in reality these motions are coupled. The computation of the $3N - 6$ modes in $H_2@C_{60}$ and related endohedral complexes was complicated by the frequent appearance of imaginary modes corresponding to rotations of the endohedral substrate within the C_{60} cage (see Table S1 in the Supporting Information). While distortion of H_2 or the H_2 complex along the transition vector

(74) Sartori, E.; Ruzzi, M.; Turro, N. J.; Komatsu, K.; Murata, Y.; Lawler, R. G.; Buchachenko, A. L. *J. Am. Chem. Soc.* **2008**, *130*, 2221–2225.
(75) Hernández-Rojas, J.; Ruiz, A.; Bretón, J.; Llorente, J. M. G. *Int. J. Quantum Chem.* **1997**, *65*, 655–663.
(76) Xu, M.; Sebastianelli, F.; Bačić, Z.; Lawler, R.; Turro, N. J. *J. Chem. Phys.* **2008**, *128*, 011101.
(77) (a) Cross, R. J. *J. Phys. Chem. A* **2008**, *112*, 7152–7156. (b) Cross, R. J. *J. Phys. Chem. A* **2001**, *105*, 6943–6944.
(78) Xu, M.; Sebastianelli, F.; Bačić, Z.; Lawler, R.; Turro, N. J. *J. Chem. Phys.* **2008**, *129*, 064313.
(79) Frisch, M. J.; et al. *Gaussian03*, revision D.01; Gaussian, Inc.: Wallingford, CT, 2004.
(80) Zhao, Y.; Truhlar, D. G. *J. Chem. Theory Comput.* **2006**, *2*, 364–382.
(81) Zhao, Y.; Truhlar, D. G. *J. Phys. Chem. A* **2006**, *110*, 10478–10486.
(82) Zhao, Y.; Truhlar, D. G. *Org. Lett.* **2006**, *8*, 5753–5755.
(83) Zhao, Y.; Truhlar, D. G. *J. Chem. Theory Comput.* **2007**, *3*, 289–300.
(84) Neese, F. *ORCA: An Ab Initio, DFT, and Semiempirical Electronic Structure Package*, version 2.6, revision 4; Max-Planck Institut für Bioanorganische Chemie: Mülheim, Germany, 2007.
(85) (a) Grimme, S. *J. Chem. Phys.* **2003**, *118*, 9095–9102. (b) Schwabe, T.; Grimme, S. *Acc. Chem. Res.* **2008**, *41*, 569–579.
(86) (a) Distasio, R. A., Jr.; Head-Gordon, M. *Mol. Phys.* **2007**, *105*, 1073–1083. (b) Takatani, T.; Sherrill, C. D. *Phys. Chem. Chem. Phys.* **2007**, *9*, 6106–6114. (c) Bachorz, R. A.; Bischoff, F. A.; Höfener, S.; Klopper, W.; Ottiger, P.; Leist, R.; Frey, J. A.; Leutwyler, S. *Phys. Chem. Chem. Phys.* **2008**, *10*, 2758–2766.
(87) (a) Bylaska, E. J.; et al. *NWChem: A Computational Chemistry Package for Parallel Computers*, version 5.0; Pacific Northwest National Laboratory: Richland, WA, 2006. (b) Kendall, R. A.; Apra, E.; Bernholdt, D. E.; Bylaska, E. J.; Dupuis, M.; Fann, G. I.; Harrison, R. J.; Ju, J.; Nichols, J. A.; Nieplocha, J.; Straatsma, T. P.; Windus, T. L.; Wong, A. T. *Comput. Phys. Commun.* **2000**, *128*, 260.
(88) Zhao, Y.; Truhlar, D. G. *Theor. Chem. Acc.* **2008**, *120*, 215–241. Erratum: Zhao, Y.; Truhlar, D. G. *Theor. Chem. Acc.* **2008**, *119*, 525.
(89) Zhao, Y.; Truhlar, D. G. *Acc. Chem. Res.* **2008**, *41*, 157–167.
(90) van Duijneveldt, F. B.; van Duijneveldt-van de Rijdt, J. G. C. M.; van Lenthe, J. H. *Chem. Rev.* **1994**, *94*, 1873–1885.
(91) (a) Hoffmann, R. *J. Chem. Phys.* **1968**, *49*, 3739–3740. (b) Woodward, R. B.; Hoffmann, R. *The Conservation of Orbital Symmetry*; Verlag Chemie: Weinheim, Germany, 1970. (c) Wright, J. S. *Can. J. Chem.* **1975**, *53*, 549–555.
(92) Gimarc, B. M. *J. Chem. Phys.* **1970**, *53*, 1623–1627.
(93) Dixon, D. A.; Stevens, R. M.; Herschbach, D. R. *Faraday Discuss. Chem. Soc.* **1977**, *62*, 110–126.
(94) Taylor, P. R.; Kormornicki, A.; Dixon, D. A. *J. Am. Chem. Soc.* **1989**, *111*, 1259–1262.
(95) Jiao, H.; Schleyer, P. v. R.; Glukhovtsev, M. N. *J. Phys. Chem.* **1996**, *100*, 12299–12304.
(96) (a) Weinhold, F. *Valency and Bonding: A Natural Bond Orbital Donor-Acceptor Perspective*; Cambridge University Press: Cambridge, U.K., 2005. (b) Reed, A. E.; Curtiss, L. A.; Weinhold, F. *Chem. Rev.* **1988**, *88*, 899–926.

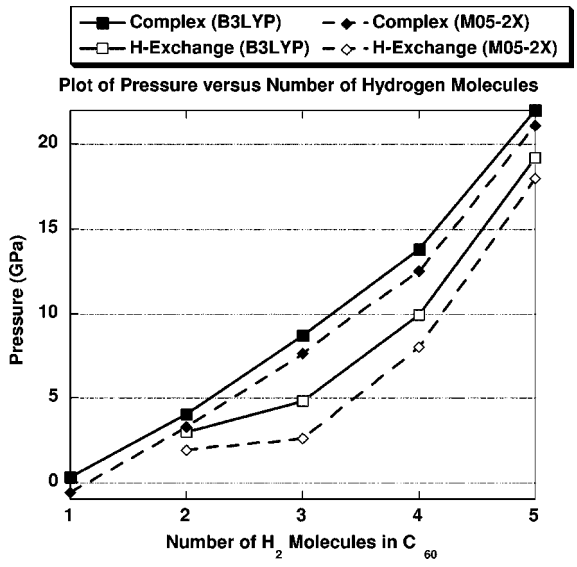

Figure 2. Plot of pressure (GPa) vs number of H_2 molecules in C_{60} for the $n H_2@C_{60}$ complexes and for the transition states for hydrogen exchange ($n H_2@C_{60}$TS) for the B3LYP/6-31G(d,p) and M05-2X/6-31G(d,p) optimized geometries. Pressures were calculated using eq 1.

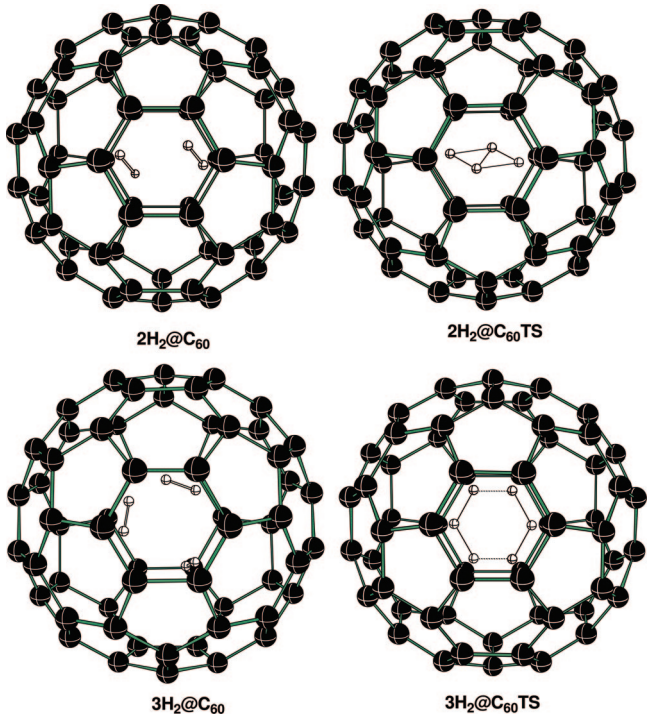

Figure 3. Molecular plot of the reactants and transition states for endohedral hydrogen exchange in $2H_2@C_{60}$ and $3H_2@C_{60}$ optimized at the B3LYP/6-31G(d,p) level.

would sometimes reduce the energy by a very small amount (<0.1 kcal/mol), one or two imaginary frequencies (corresponding to nH_2 rotation) would often remain. For example, reducing the symmetry of $H_2@C_{60}$ from D_{2h} to C_i changed the energy, ZPC, and heat capacity correction by 0.05, 0.02, and 0.01 kcal/mol, respectively [B3LYP/6-31G(d,p)], and increased the entropy by 2.9 cal mol^{-1} K^{-1}; the number of imaginary frequencies remained constant. For $4H_2@C_{60}$, reducing the symmetry from C_{2v} to C_2 reduced the energy by 0.9 kcal/mol and the number of imaginary modes from four to zero. However, in this case, the largest imaginary mode (309i) corresponded to

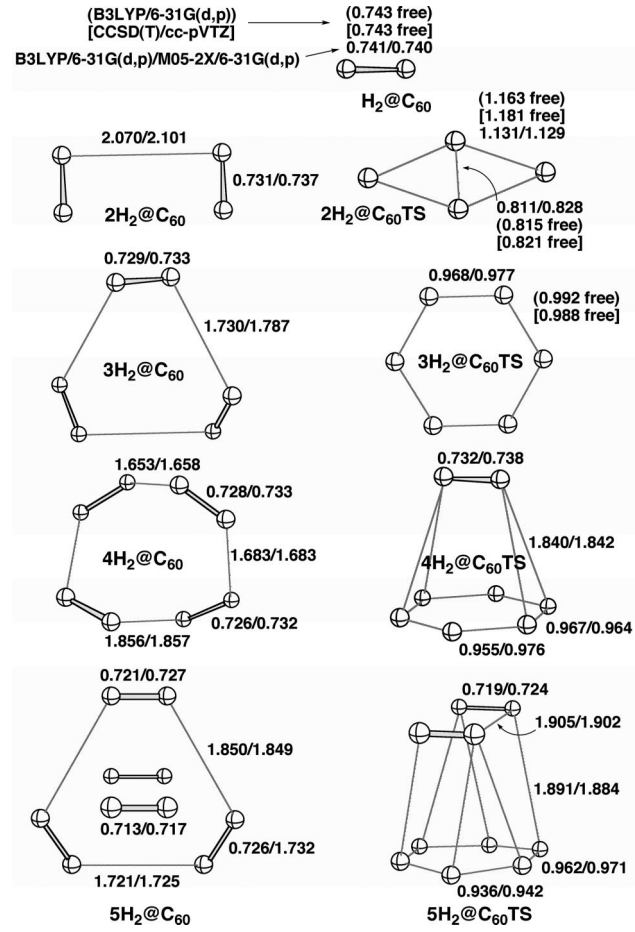

Figure 4. Molecular plots of the hydrogen atoms for $n H_2@C_{60}$ and $n H_2C_{60}$TS ($n = 1-5$). The carbon atoms of the C_{60} cage have been omitted for clarity. The first values without parentheses are for endohedral species optimized at the B3LYP/6-31G(d,p) level, while the values following the slashes are for endohedral species optimized at the M05-2X/6-31G(d,p) level. The geometries of the hydrogen exchange in free $2H_2$ and $3H_2$ at the B3LYP/6-31G(d,p) and CCSD(T)/cc-pVTZ levels are also shown. Values for free $2H_2$ and $3H_2$ are given in parentheses for B3LYP/6-31G(d,p) and in brackets for CCSD(T)/cc-pVTZ.

a distortion within the $4H_2$ cluster. For all of the endohedral clusters considered, the zero-point energies and integrated heat capacities were very similar for the complex and the transition state for hydrogen exchange [see Table S1 in the Supporting Information for total energies, zero-point energies, heat capacity corrections, entropies, and low-frequency modes at the B3LYP/6-31G(d,p) and M05-2X/6-31G(d,p) levels]. For that reason, zero-point and heat capacity corrections to 298 K were not applied to the hydrogen exchange barriers. Also, the contribution of the $-T\Delta S$ term to the hydrogen free energy barrier, which varied from almost zero for $4H_2@C_{60}$ to 4.5 kcal/mol for $5H_2@C_{60}$, was much smaller than the $-T\Delta S$ term for the free hydrogen exchange in $3H_2$. Given the uncertainty of the computed low-frequency modes in the endohedral complexes and transition states, the $-T\Delta S$ contribution to the hydrogen exchange free energy barriers was not included.

The pressures in the endohedral clusters and transition states ($n H_2@C_{60}$ and $n H_2@C_{60}$TS), which were calculated using eq 1, are given in Table 4 and Figure 2. The method used to calculate pressure requires the gradients (forces) to be calculated for the cage with the hydrogen molecules removed. Different values were obtained from the B3LYP/6-31G(d,p) and M05-2X/6-31G(d,p) methods using the geometries optimized at the

Table 5. Energy Terms (kcal/mol) Relative to $nH_2 + C_{60}$ at Different Levels of Theory for Structures Optimized at the B3LYP/6-31G(d,p) Level

	C_{60} distort	nH_2 distort	total distortion	TIE	FFI	BSSE	FFI+BSSE	TIE+BSSE	H-exchange[a]
				MP2/cc-pVDZ					
$H_2@C_{60}$	0.12	0.02	0.14	−5.63	−5.77	2.27	−3.50	−3.36	
$2H_2@C_{60}$	−0.30	5.97	5.67	0.88	−4.79	7.02	2.23	7.90	
$3H_2@C_{60}$	−0.63	16.71	16.08	14.24	−1.04	11.88	10.84	26.12	0.0
$3H_2@C_{60}$TS	−0.66	66.03	65.37	48.83	−16.54	10.18	−6.36	59.01	32.89
$3H_2$TS[b]		65.53							
$4H_2@C_{60}$	−1.15	28.77	27.62	30.56	2.94	16.91	19.85	47.47	
$5H_2@C_{60}$	−0.63	51.60	50.97	70.04	19.07	22.31	41.38	92.35	
				SCS-MP2/cc-pVDZ					
$H_2@C_{60}$	1.79	0.02	1.81	−2.59	−4.40	3.91	−0.49	1.32	
$2H_2@C_{60}$	−0.51	6.05	5.54	5.06	−0.48	6.77	6.29	11.83	0.0
$2H_2@C_{60}$TS	−0.48	110.20	109.72	100.28	−9.44	6.81	−2.63	107.09	95.26
$3H_2@C_{60}$	−1.03	17.28	16.25	21.78	5.53	11.46	16.99	33.24	0.0
$3H_2@C_{60}$TS	−0.91	71.18	70.27	59.70	−10.57	9.76	−0.81	69.46	36.22
$3H_2$TS[b]		70.57							
$4H_2@C_{60}$	−1.66	29.96	28.30	41.66	13.36	16.28	29.64	57.94	0.0
$4H_2@C_{60}$TS	−1.76	79.29	77.53	73.66	−3.87	11.88	8.01	85.54	27.60
$5H_2@C_{60}$	−1.58	53.34	51.76	84.89	33.13	16.24	49.37	101.13	0.0
$5H_2@C_{60}$TS	−1.95	102.02	100.07	118.45	18.38	15.74	34.12	134.19	33.06
				B3LYP/cc-pVDZ[c]					
$H_2@C_{60}$	−3.22	0.04	−3.18	−1.54	1.64	0.60	2.24	0.70	
$2H_2@C_{60}$	−2.90	5.86	2.96	16.63	13.67	2.26	15.93	18.89	0.0
$2H_2@C_{60}$TS	−3.22	98.10	94.88	105.59	10.71	2.24	12.95	107.83	88.94
$3H_2@C_{60}$	−2.54	15.21	12.67	41.60	28.93	3.78	32.71	45.38	0.0
$3H_2@C_{60}$TS	−3.21	55.74	52.53	69.64	17.11	2.60	19.71	72.24	26.86
$3H_2$TS[b]		55.62							
$4H_2@C_{60}$	−2.28	26.42	24.14	70.27	46.13	5.41	51.54	75.68	0.0
$4H_2@C_{60}$TS	−2.87	63.52	60.65	94.63	33.98	3.92	37.90	98.55	22.87
$5H_2@C_{60}$	−0.29	49.10	48.81	123.69	74.88	7.23	82.11	130.92	0.0
$5H_2@C_{60}$TS	−1.26	85.76	84.50	150.63	66.13	5.90	72.03	156.53	25.61
$3H_2@C_{70}$				1.71					0.0
$3H_2@C_{70}$TS				59.05					57.34[d]
$3H_2@C_{82}$				−8.79					0.0
$3H_2@C_{82}$TS				55.42					64.21[d]
				M05-2X/cc-pVDZ					
$H_2@C_{60}$	0.07	0.03	0.10	−6.16	−6.26	0.45	−5.81	−5.71	
$2H_2@C_{60}$	0.79	5.54	6.33	3.38	−2.95	1.89	−1.06	5.27	0.0
$2H_2@C_{60}$TS	0.49	103.03	103.52	95.52	−8.00	1.87	−6.13	97.39	92.12
$3H_2@C_{60}$	0.68	14.26	14.94	20.28	5.34	3.27	8.61	23.55	0.0
$3H_2@C_{60}$TS	1.95	60.80	62.75	54.59	−8.16	2.11	−6.05	56.70	33.15
$3H_2$TS[b]		59.98							
$4H_2@C_{60}$	2.90	23.75	26.65	39.93	13.28	4.58	17.86	44.51	0.0
$4H_2@C_{60}$TS	1.74	65.88	67.62	69.33	1.71	3.45	5.16	72.78	28.27
$5H_2@C_{60}$	6.28	44.56	50.84	85.44	34.60	5.99	40.59	91.43	0.0
$5H_2@C_{60}$TS	4.86	87.29	92.15	117.75	25.60	5.16	30.76	122.91	31.48

[a] The H-exchange barrier is computed as the difference between the TIE+BSSE values for $nH_2@C_{60}$TS and $nH_2@C_{60}$. [b] Difference between the energies of the "free" TS (D_{6h}) and $3H_2$. [c] The FFI values at the B3LYP/6-31G(d,p) level are very similar to the corresponding values at the B3LYP/cc-pVDZ level. For $H_2@C_{60}-5H_2@C_{60}$TS the values are: 1.49, 13.81, 9.61, 28.86, 16.31, 46.18, 32.67, 75.24, and 64.79 kcal/mol, respectively. [d] The hydrogen exchange barriers for $3H_2@C_{70}$ and $3H_2@C_{82}$ do not include the counterpoise correction.

Table 6. Estimation of Contributions (kcal/mol) to the Lowering of the $3H_2 \rightarrow$ TS Free Energy Barrier at 298 K in Going from the "Free" Exchange Reaction to the Reaction within the C_{60} Cage

method/cc-pVDZ	intracluster repulsion	cage-cluster dispersion	$-T\Delta S$ [c]	sum (estimated $\Delta\Delta G^{\ddagger}$)	calculated $\Delta\Delta G^{\ddagger}$
MP2	16.21[a]	17.20[b]	17.68	51.05	50.30[d]
B3LYP	15.33	11.82	17.68	44.83	45.24
M05-2X	15.08	14.66	17.68	47.42	44.49
M06-2X	16.10	16.37	17.68	50.15	47.03
RI-SCS-MP2	17.89	17.71	17.68	53.28	52.01

[a] For example: MP2 = 16.71 + 65.53 − 66.03 = 16.21 (Table 5). [b] For example: MP2 = 10.84 + 6.36 = 17.20 (Table 5). [c] The "$-T\Delta S$" term comes from the free $3H_2$ exchange at the B3LYP/6-31G(d,p) level. The calculated $-T\Delta S$ contribution for $3H_2$ exchange within the C_{60} cage is small (assumed to be zero). [d] For example: MP2 = (65.53, Table 5) − (66.93, Table 2) + (84.61, Table 2) − (32.89, Table 5) = 50.30.

respective levels. Thus, the pressure computed at the M05-2X/6-31G(d,p) level is less than that at the B3LYP/6-31G(d,p) level for a given cluster or transition state as a result of the better description of dispersion by M05-2X, which moderates repulsion. For every cluster, the pressure exerted by the $nH_2@C_{60}$ cluster is greater than the pressure exerted by the transition state for hydrogen exchange ($nH_2@C_{60}$TS). As expected, the calculated pressure reflects the total interaction energy (TIE) between the nH_2 cluster and the C_{60} cage; the greater the repulsion, the greater the pressure. As the number of H_2 molecules increases,

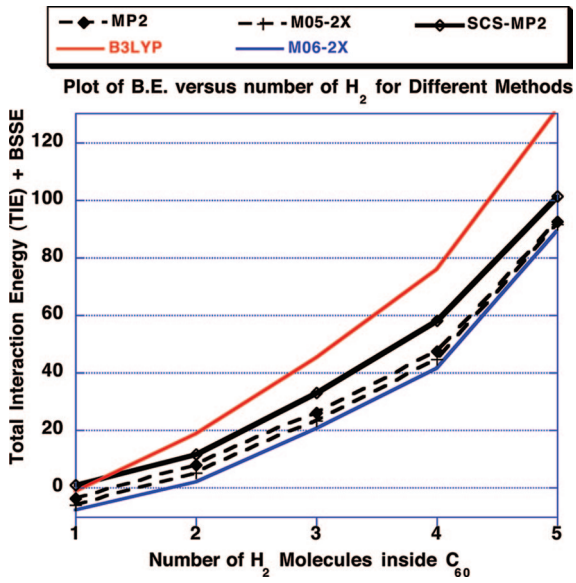

Figure 5. Plot of TIE+BSSE (from Table 5) versus the number of H_2 molecules in the C_{60} cage for different methods, using the B3LYP/6-31G(d,p) optimized geometries.

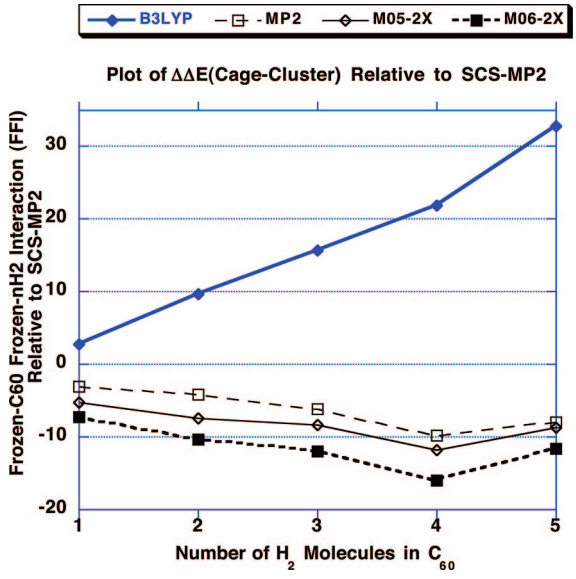

Figure 6. Plot of FFI+BSSE values for various methods (from Table 5) relative to the SCS-MP2 value versus the number of H_2 molecules in the C_{60} cage, using the B3LYP/6-31G(d,p) optimized geometries.

the pressure increases. For a given cluster, as the cage size increases ($3H_2@C_{60} \rightarrow 3H_2@C_{70} \rightarrow 3H_2@C_{82}$), the pressure decreases (8.7 → 4.7 → 1.5 GPa).

Molecular plots of $2H_2@C_{60}$ and $3H_2@C_{60}$ and the corresponding transition states for hydrogen exchange ($2H_2@C_{60}$TS and $3H_2@C_{60}$TS) are shown in Figure 3. A comparison of the molecular parameters of the nH_2 clusters and the hydrogen exchange transition states is made in Figure 4, in which the carbon atoms have been omitted for clarity. In addition, values at the B3LYP/6-31G(d,p) and CCSD(T)/cc-pVTZ levels are given for the free hydrogen exchange transition states ($2H_2$TS and $3H_2$TS). As the number of H_2 molecules inside the C_{60} cage increases, increased repulsion between the cage and the hydrogen cluster causes the H−H bond distances to decrease.

An analysis of the nH_2/C_{60} interactions in the endohedral complexes and transition states along with a comparison of

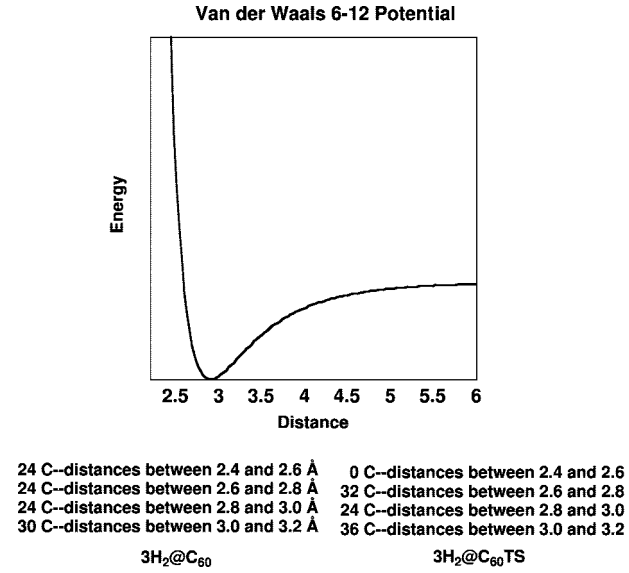

Figure 7. Plot of the van der Waals potential curve with a minimum (2.9 Å) at the sum of the van der Waals radii for H (1.2 Å) and C (1.7 Å). The values listed below the plot indicate the numbers of contacts [using B3LYP/6-31G(d,p) geometries] between H and C in the indicated ranges for $3H_2@C_{60}$ and $3H_2@C_{60}$TS. The units on the distance axis are Angstroms.

different methods (MP2, SCS-MP2, B3LYP, and M05-2X) is given in Table 5 (values for M06-2X, which are similar to those for M05-2X, are available in Table S2 in the Supporting Information). The first three columns give the distortion energies of C_{60} (i.e., energies using the C_{60} atom positions in $nH_2@C_{60}$ relative to the energy for free C_{60}) and nH_2 (i.e., energies using the nH_2 positions $nH_2@C_{60}$ relative to those for n H_2 molecules) and their sum. The row labeled "$3H_2$TS" gives the energy of the $3H_2$ exchange transition state relative to that of three H_2 molecules. The very similar energy of nH_2 for $3H_2@C_{60}$TS and $3H_2$TS (66.03 vs 65.53, MP2, Table 5) indicates that the C_{60} cage does not "squeeze" the transition state. The "TIE" column gives the total interaction energy, which is simply equal to $E_{nH_2@C_{60}} - E_{n\cdot H_2} - E_{C_{60}}$, while the "FFI" column gives the frozen-C_{60} frozen-nH_2 interaction energy (FFI), which represents the attractive (negative) or repulsive (positive) interaction between the frozen C_{60} cage and the frozen nH_2 cluster. The column labeled "BSSE" gives the basis set superposition error calculated using the counterpoise method. The "FFI+BSSE" column (the sum of the FFI and BSSE) represents the interaction of frozen C_{60} and frozen nH_2 corrected for BSSE, while the "TIE+BSSE" column (the sum of the TIE and BSSE) is the BSSE-corrected binding with respect to n H_2 molecules and relaxed C_{60}. The "H-exchange" column gives the BSSE-corrected barrier for hydrogen exchange, in which zero-point and heat capacity corrections have not been included because they are expected to be small.

In contrast to the C_{60} distortion energy, the energy to squeeze n H_2 molecules together is quite large and increases as n increases. For a particular value of n, the distortion energy for nH_2 (i.e., $nH_2@C_{60}$) is much larger for the complex than the "extra" distortion beyond that required to squeeze the hydrogen molecules into the hydrogen exchange transition state (i.e., $nH_2@C_{60}$TS − nH_2TS). Thus, the distortion of the n H_2 molecules that is needed to reach the transition state reduces the repulsion between the hydrogen atoms and the interior of the C_{60} cage. For example, the TIE+BSSE value is 32.89 kcal/

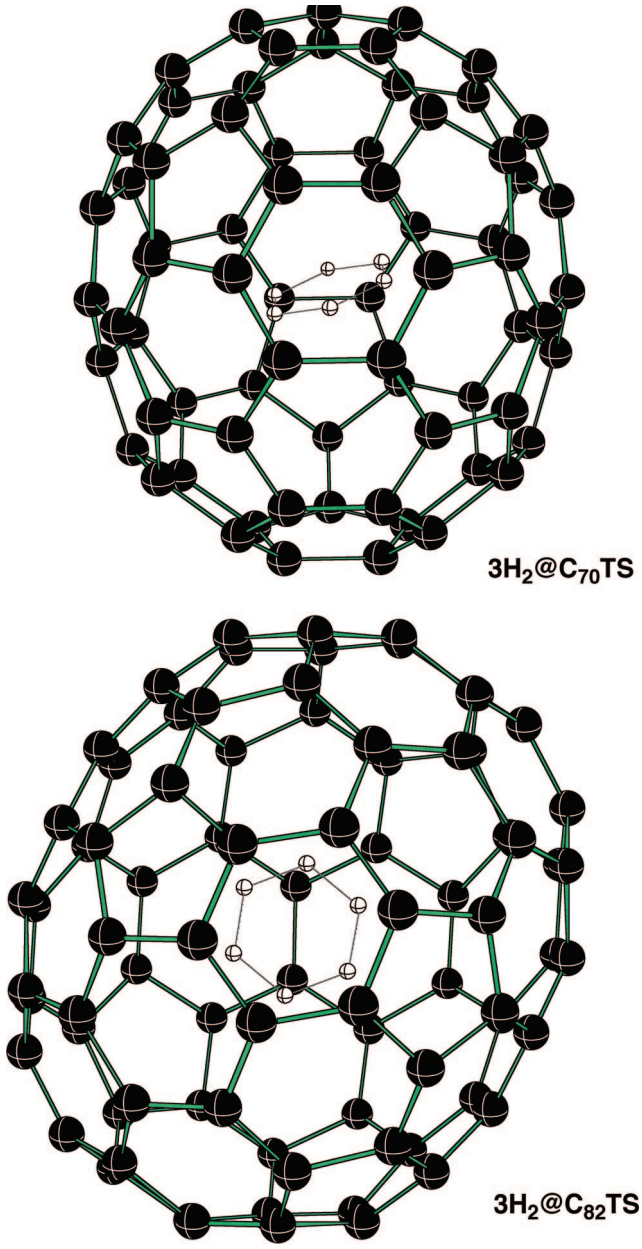

Figure 8. Molecular plots of the transition states for hydrogen exchange inside C_{70} and C_{82} cages ($3H_2@C_{70}$TS and $3H_2@C_{82}$TS).

mol greater for $3H_2@C_{60}$TS than for $3H_2@C_{60}$ (59.01 vs 26.12 kcal/mol, MP2, Table 5). The interaction of the frozen C_{60} with the frozen nH_2 is a measure of steric repulsion moderated by dispersion. Thus, while the TIE of $3H_2$ with C_{60} is 14.24 kcal/mol using MP2, it is 41.60 with B3LYP, a DFT method which is known to underestimated dispersion effects. A plot of TIE+BSSE versus the number of H_2 molecules for several computational methods (Figure 5) shows that the binding is attractive for one H_2 molecule but quickly becomes repulsive as the number of H_2 molecules increases. If one plots the FFI+BSSE value for each method relative to that for SCS-MP2[85,86] versus the number of H_2 molecules (Figure 6), it is clear that the repulsion increases much more rapidly at the B3LYP level than at the SCS-MP2 level. The other three computational methods (MP2, M05-2X, M06-2X) calculate increases in repulsion energy similar to that for SCS-MP2. If it is assumed that B3LYP gives no dispersion energy, it appears that dispersion reduces the repulsion by ~7 kcal/mol per added H_2.

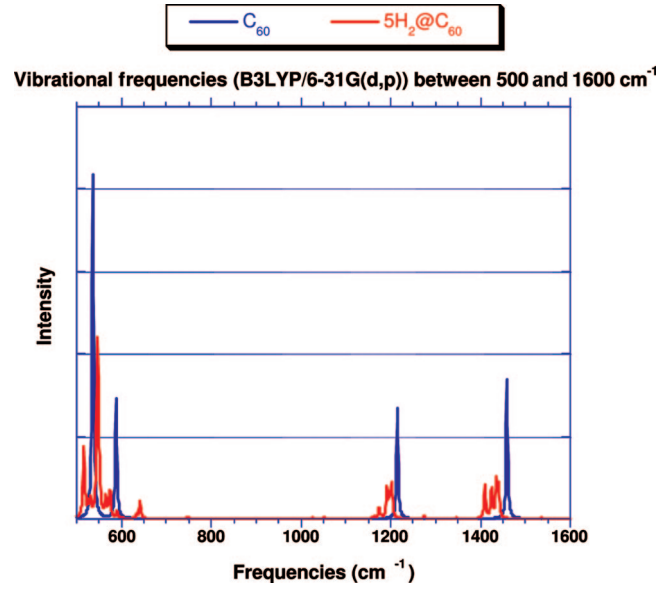

Figure 9. Comparison of calculated [B3LYP/6-31G(d,p)] vibrational frequencies in the 500−1600 cm^{-1} range for C_{60} (blue) and $5H_2@C_{60}$ (red).

The counterpoise correction varies from 2 to 22 kcal/mol for MP2 and from 1 to 7 kcal/mol for B3LYP from $H_2@C_{60}$ to $5H_2@C_{60}$. It is interesting to note that the BSSE is ~3 times larger for MP2 than for B3LYP (the M05-2X and M06-2X results are similar to those for B3LYP). Since the repulsion between the transition state and the cage is less than the repulsion between the reactant nH_2 complex and the cage, the BSSE for $nH_2@C_{60}$TS is smaller than that for $nH_2@C_{60}$ for a given number of hydrogen molecules and computational method.

The calculated hydrogen exchange barriers are remarkably similar for the different computational methods (Table 5). For example, excluding the B3LYP value (26.9 kcal/mol), the $3H_2@C_{60}$ hydrogen exchange barriers only vary from 32.89 to 36.22 kcal/mol. The hydrogen exchange in $2H_2@C_{60}$ has a much larger barrier than in $3H_2@C_{60}$ (95.26 vs 36.22 kcal/mol, SCS-MP2, Table 5), which is analogous to the case of the free hydrogen exchange barriers in $2H_2$ and $3H_2$ (Table 1). For more than three H_2 molecules (i.e., for $4H_2@C_{60}$ and $5H_2@C_{60}$), the hydrogen exchange reaction mechanism is the same as for $3H_2@C_{60}$, but the barrier is much lower in energy than that for hydrogen exchange in $2H_2@C_{60}$. Thus, the number of spectator H_2 molecules has very little effect on the basic $3H_2$ exchange mechanism (36.22, 27.60, and 33.06 kcal/mol for 0, 1, and 2 spectator H_2 molecules, respectively, SCS-MP2, Table 5).

The catalytic effect of the C_{60} cage comes from three sources: (1) the compression required to fit three H_2 molecules into the cage, (2) the large dispersion interaction in the transition state, and (3) the unimolecular nature of the free hydrogen exchange. In regard to the first source of the catalytic effect, the energy (repulsion) for fitting three H_2 molecules into the C_{60} cage is much larger than that for fitting the transition state for hydrogen exchange into the cage. If one considers the H−C van der Waals curve (Figure 7), it is clear there are a greater number of repulsive H−C contacts in the reactant (24 pairs in the interval 2.4−2.6 Å) than in the transition state (none in the interval 2.4−2.6 Å). The second source, dispersion, is greater for the transition state than for the reactant. One reason is a greater number of H−C contacts in the 3.0−3.2 Å interval in the transition state than in the reactant (36 pairs compared to 30

Table 7. Calculated [B3LYP/6-31G(d,p) and M05-2X/6-31G(d,p)] H−H Distances and H_2 Stretching Frequencies in H_2 and $nH_2@C_{60}$, $3H_2@C_{70}$, and $3H_2@C_{82}$[a]

	H−H Distances (Å)				
H_2	0.743/0.741				
$H_2@C_{60}$	0.741/0.740				
$2H_2@C_{60}$	0.731/0.737	0.731/0.737			
$3H_2@C_{60}$	0.729/0.733	0.729/0.733	0.729/0.733		
$4H_2@C_{60}$	0.729/0.733	0.729/0.733	0.729/0.733	0.728/0.733	
$5H_2@C_{60}$	0.726/0.717	0.726/0.717	0.728/0.727	0.726/0.732	0.727/0.732
$3H_2@C_{70}$	0.730	0.733	0.734		
$3H_2@C_{82}$	0.736	0.737	0.738		
	H_2 Stretching Frequencies (cm^{-1})				
H_2	4466/4513				
$H_2@C_{60}$	4491/4536				
$2H_2@C_{60}$	4619/4555	4636/4573			
$3H_2@C_{60}$	4605/4587	4652/4619	4652/4619		
$4H_2@C_{60}$	4602/4565	4645/4610	4671/4631	4685/4644	
$5H_2@C_{60}$	4617/4584	4677/4635	4740/4701	4849/4847	4863/4860

[a] The B3LYP value is given first, followed by the M05-2X value. The number of entries in a row is determined by the number of H_2 molecules in the cluster.

pairs). However, an additional contribution is the smaller separation between the highest occupied nH_2 orbital (nH_2TS HOMO) in the transition state (compared with the nH_2 cluster, i.e., the nH_2 HOMO) and the lowest-energy empty orbital of the C_{60} cage (cage LUMO). The resulting donor−acceptor interaction would stabilize the endohedral hydrogen exchange transition state relative to the nH_2 cluster. The third catalytic contribution is due to entropy considerations. The free hydrogen exchange is a termolecular process with a very unfavorable entropic contribution. On the other hand, the hydrogen exchange inside C_{60} is similar to a unimolecular reaction and has a much smaller entropic contribution.

The three contributions are estimated in Table 6 for several different computational methods. The results are largely independent of method. As expected, the B3LYP method predicts a smaller contribution due to dispersion (the second catalytic contribution), but this contribution also includes the donor−acceptor stabilization, which should be properly described by the B3LYP method. The sum of the three contributions is very similar to the calculated lowering of the free energy barrier by the different methods. If one takes a 50 kcal/mol lowering of the free energy barrier for $3H_2 \rightarrow 3H_2$ caused by the C_{60} cage, one obtains a k_{cat}/k_{uncat} ratio of 10^{36} at 298 K. This value is 18 orders of magnitude greater than the largest enzymatic rate enhancement[1] (10^{36} compared to 10^{18}), a truly remarkable value!

If one assumes that a 1% conversion of $D_2/2H_2$ into $2HD/H_2$ can be experimentally detected inside C_{60} and uses an A value of 10^{11} s^{-1} and an activation barrier of 32.9 kcal/mol, the Arrhenius equation gives reaction times of 3000 years, 3 weeks, and 3 min at 298, 373, and 473 K, respectively. The C_{60} cage is stable at temperatures much higher than 473 K, which suggests that if $3H_2@C_{60}$ (and the corresponding $D_2/2H_2@C_{60}$) can be made, then the conversion should be easily observed.

The effect of increasing the size of the cage on the hydrogen exchange barrier was also explored by considering $3H_2@C_{70}$ and $3H_2@C_{82}$. Because of the sizes of these systems, vibrational frequencies and counterpoise corrections were not calculated for the complexes or hydrogen exchange transition states. Carrying out the reaction in a larger fullerene cage should make the reaction more similar to the free exchange reaction. Indeed, the hydrogen exchange barriers in C_{70} and C_{82} are 57.34 and 64.21 kcal/mol, respectively, which are close to the free hydrogen exchange barrier of 61.7 kcal/mol at the B3LYP/6-31G(d,p) level (Table 2). Three H_2 molecules can fit into C_{70} and C_{82} with 39.89 and 50.39 kcal/mol less repulsion than into C_{60}, respectively. The molecular plots of $3H_2@C_{70}$TS and $3H_2@C_{82}$TS (Figure 8) show that these hydrogen-exchange transition states are very similar to $3H_2@C_{60}$TS.

The vibrational frequencies of the C−C modes in C_{60} and $5H_2@C_{60}$ are compared in Figure 9. It is interesting that the C−C modes of $5H_2@C_{60}$ below 600 cm^{-1} are at higher frequency while those near 1200 cm^{-1} and above are at lower lower frequency. The lower frequencies of the stretching modes in $5H_2@C_{60}$ are probably a result of C−C bond weakening due to stretching.

In 1991, Cioslowski[35] used the HF/4-31G method to compute a 1.2 kcal/mol stabilization energy of H_2 in C_{60}, a 95 cm^{-1} shift toward higher frequencies (blue shift, 4592 → 4687 cm^{-1}), and a 0.003 Å reduction in the H−H distance. The present calculations at the B3LYP/6-31G(d,p) (M05-2X/6-31G(d,p)) level are similar: a 1.5 (6.2) kcal/mol stabilization energy (without BSSE correction), a 25 (16) cm^{-1} blue shift, and a 0.002 (0.001) Å reduction in the H−H distance. Cioslowski and more recently Shameema et al.[37] computed a small blue shift for HF embedded in C_{60}. The latter authors indicated that the stabilization is due to dispersion and that the blue shift arises from confinement. Ramachandran and Sathyamurthy[49] found that when one water was embedded in C_{60}, the blue shift in the symmetric OH stretch (HF/6-31G level with a 0.8929 scaling factor) was 44 cm^{-1}, which increased to 69 cm^{-1} when two water molecules were embedded in C_{60}. The interaction energy (MP2/6-31G//HF/6-31G) was −9.9 kcal/mol with one water and 24.5 kcal/mol for two waters.[49]

A comparison of the H−H bond distances and stretching frequencies calculated at the B3LYP/6-31G(d,p) and M05-2X/6-31G(d,p) levels is made in Table 7. As the number of H_2 molecules increases, the H−H bond lengths decrease and the H−H stretching frequency increases. The average blue shift and H−H bond length reduction for $nH_2@C_{60}$ as n increases from 1 to 5 are reported in Table 8. The blue shift is less for M05-2X than for B3LYP, and both steadily increase as the number of H_2 molecules in the C_{60} cage increases. In contrast to the experimental red shift (90 cm^{-1}) reported by Carravetta and coworkers[69] for $H_2@C_{60}$, the present calculations predict a blue shift of 25 and 23 cm^{-1} at the B3LYP/6-31G(d,p) and M05-2X/6-31G(d,p) levels, respectively (Table 8). Molecular hydrogen has a rather large anharmonic contribution[97] of 239 cm^{-1} (4161 → 4400 cm^{-1}). It is possible that the anharmonic correction to the calculated harmonic frequency of $H_2@C_{60}$ is even larger, which might resolve the experiment−theory dis-

Table 8. Average Blue Shift (cm^{-1}) and H−H Bond Reduction (Å) of nH_2 in C_{60}[a]

	$\Delta\nu_{H_2}$	Δ(H−H)
$H_2@C_{60}$	25 (23)[b]	−0.002 (−0.001)
$2H_2@C_{60}$	162 (52)	−0.012 (−0.004)
$3H_2@C_{60}$	170 (95)	−0.014 (−0.008)
$4H_2@C_{60}$	185 (99)	−0.014 (−0.008)
$5H_2@C_{60}$	283 (212)	−0.016 (−0.016)

[a] The B3LYP/6-31G(d,p) value is given first, followed by the M05-2X/6-31G(d,p) value in parentheses. [b] A blue shift of 90 cm^{-1} was calculated at the HF/4-31G(C)/DZP(H_2) level (see ref 35).

crepancy. The endohedral H−H potential is expected to be similar to that of H_2 during contraction. However, the dispersion forces between H_2 and the interior of the C_{60} cage when the H−H bond elongates could make the potential more anharmonic than in free H_2.

Conclusions

The fullerene cages C_{60}, C_{72}, and C_{82} were considered as molecular containers for the hydrogen exchange reaction $3H_2 \rightarrow 3H_2$. The interaction energies and counterpoise corrections were compared for the MP2, SCS-MP2, B3LYP, M05-2X, and M06-2X methods. The B3LYP method was found to significantly underestimate dispersion interactions. In contrast to previous studies, the present study considers dispersion as reducing (moderating) the repulsion between nH_2 and the cage rather than as an attractive interaction.

When two H_2 molecules are enclosed in C_{60}, the hydrogen exchange barrier is very high. However, when three H_2 molecules are enclosed in C_{60}, a much lower hydrogen exchange barrier through a six-membered transition state is possible. For four or more H_2 molecules, the lowest hydrogen exchange barrier is still through a six-membered H-ring in which the other H_2 molecule(s) act as innocent bystander(s). The C_{60} cage reduces the free energy of the hydrogen exchange over the reaction outside of the ring by (1) raising the reactant energy by compression, (2) reducing the enengy of the transition state by dispersion, and (3) changing the termolecular reaction into a unimolecular reaction within the C_{60} cage. The sum of the three effects is ∼50 kcal/mol, which gives a k_{cat}/k_{uncat} ratio of 10^{36}. Thus, Cioslowski's description[35] of the endohedral complexes as "polarizable spheres of carbon atoms with freely tumbling guest molecules 'suspended' inside" appears to be accurate.

Acknowledgment. The Alabama Supercomputer Center is acknowledged for a generous grant of computer time.

Note Added in Proof. The synthesis of the endohedral complex $2H_2@C_{70}$ has recently been reported.[98]

Supporting Information Available: Absolute energies, zero-point energies, heat capacity corrections, entropies, and low-frequency modes at the B3LYP/6-31G(d,p) and M05-2X/6-31G(d,p) levels (Table S1); data for M06-2X in the same format as in Table 5 (Table S2); complete refs 79 and 87; and optimized Cartesian coordinates [B3LYP/6-31G(d,p)] of $nH_2@C_{60}$ and $nH_2@C_{60}$TS species (Table S3). This material is available free of charge via the Internet at http://pubs.acs.org.

JA8071868

(97) (a) Huber, K. P.; Herzberg, G. *Molecular Spectra and Molecular Structure IV: Constants of Diatomic Molecules*; Van Nostrand Reinhold: New York, 1979. (b) Stoicheff, B. P. *Can. J. Phys.* **1957**, *35*, 730.

(98) Murata, M.; Maeda, S.; Morinaka, Y.; Murata, Y.; Komatsu, K. *J. Am. Chem. Soc.* **2008**, *130*, 15800–15801.